Toward Single-Enzyme Molecule Electrochemistry: [NiFe]-Hydrogenase Protein Film Voltammetry at Nanoelectrodes

Freek J. M. Hoeben,[§] F. Stefan Meijer,[§,†] Cees Dekker,[§] Simon P. J. Albracht,[‡] Hendrik A. Heering,[§,⊥,*] and Serge G. Lemay[§,*]

[§]Kavli Institute of Nanoscience, Delft University of Technology, Lorentzweg 1, 2628 CJ Delft, The Netherlands, [‡]Swammerdam Institute for Life Sciences, University of Amsterdam, Nieuwe Achtergracht 166, 1018 WV Amsterdam, The Netherlands, and [⊥]Leiden Institute of Chemistry, Leiden University, Einsteinweg 55, 2333 CC Leiden, The Netherlands. [†]Stefan Meijer passed away shortly after initiating this research.

ABSTRACT We have scaled down electrochemical assays of redox-active enzymes enabling us to study small numbers of molecules. Our approach is based on lithographically fabricated Au nanoelectrodes with dimensions down to *ca.* 70 × 70 nm^2. We first present a detailed characterization of the electrodes using a combination of scanning electron microscopy, cyclic voltammetry, and finite-element modeling. We then demonstrate the viability of the approach by focusing on the highly active [NiFe]-hydrogenase from *Allochromatium vinosum* immobilized on polymyxin-pretreated Au. Using this system, we successfully demonstrate a distinct catalytic response from less than 50 enzyme molecules. These results strongly suggest the feasibility of using bioelectrochemistry as a new tool for studying redox enzymes at the single-molecule level.

KEYWORDS: nanofabrication · nanoelectrodes · redox enzymes · [NiFe]-hydrogenase · cyclic voltammetry · protein film voltammetry · finite-element modeling

Many of the most exciting recent developments in enzymatic studies have resulted from an increasing ability to probe the internal dynamics of individual molecules. Most existing single-molecule techniques exploit either fluorescence or mechanical transduction to couple to the enzyme molecule.[1] Developing qualitatively new ways of probing single-enzyme molecules would extend the diversity of molecular species and phenomena that can be studied at the single-molecule level. We are particularly interested in redox enzymes, which catalyze electron-transfer reactions. An ideal tool to study these enzymes is protein film voltammetry (PFV),[2,3] in which redox-active enzymes are immobilized on a suitable electrode material so as to yield an electronic contact between the active site of the protein and the electrode. The electrode potential is modulated, thus controlling the chemistry of the active site, and the catalytic activity of the enzyme is monitored by detecting the electrical current flowing through the electrode. PFV represents an indispensable technique for studying the mechanistic and kinetic properties of redox enzymes. However, due to the relatively large electrode dimensions used (typically in the μm^2 to mm^2 range), PFV inevitably probes the characteristics of large ensembles of enzyme molecules. Consequently, it averages out variations resulting from molecular conformational fluctuations or attachment mode[4] as well as any slow dynamics of individual molecules in the ensemble. Overcoming these limitations requires scaling down PFV to the level of a single-enzyme molecule, an experimental challenge that has not been met to date.

Single-enzyme molecule voltammetry, sketched in Figure 1, is conceptually simple but presents several significant experimental hurdles. First, a suitable method must be developed to immobilize the enzyme while retaining catalytic activity. This is a requirement common to bulk PFV, but work at the single-molecule level renders it even more critical. Second, the measurement equipment must be sufficiently sensitive to detect the extremely small electrical currents associated with the catalytic activity of a single-enzyme molecule. Lastly, the background current from reactions not associated with catalytic activity of the enzyme must be sufficiently suppressed to allow discerning the desired signal.

Here we demonstrate the scaling down of PFV to a small number of enzyme molecules. Our approach is based on

See the accompanying Perspective by Bard on p 2437.

*Address correspondence to h.a.heering@chem.leidenuniv.nl, s.g.lemay@tudelft.nl.

Received for review August 15, 2008 and accepted October 18, 2008.

Published online November 4, 2008. 10.1021/nn800518d CCC: $40.75

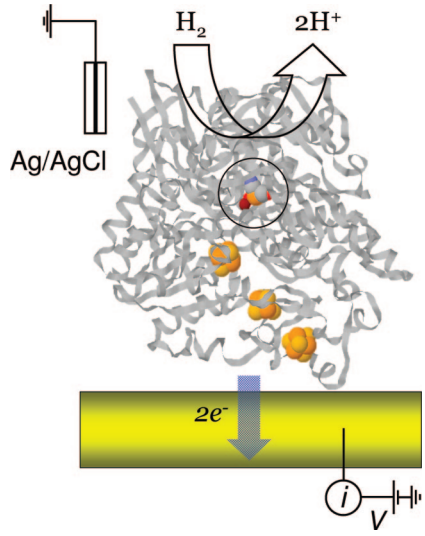

Figure 1. Schematic illustration depicting a single redox-active enzyme molecule adhered to a nanosized electrode. Modulation of the electrode potential (*V*) determines the chemistry of the active site (circled), which is electronically connected to the electrode by an electron-transfer chain of prosthetic groups. The arrows illustrate the H_2 oxidation activity of a single *Av* H_2ase molecule (based on the structure of *Desulfovibrio gigas* [NiFe]-hydrogenase,[13] which is highly similar to that of *Av* H_2ase).[14]

lithographically fabricated nanoscale Au electrodes. By virtue of their small surface area, nanoelectrodes lead to reduced background Faraday currents, which greatly facilitates detecting the activity of a small number of enzyme molecules. Additional advantages include decreased capacitance due to the decrease in electrode surface area, fast establishment of a steady-state signal, and enhanced mass transport to the electrode.[5,6] For these experiments, we have selected the [NiFe]-hydrogenase from *Allochromatium vinosum* (*Av* H_2ase). This enzyme reversibly interconverts molecular hydrogen into protons and electrons. Its electrochemical signature has been extensively characterized,[7−9] and its catalytic activity has been demonstrated to be of the same order as that of a Pt catalyst.[10] Its estimated maximum turnover rate of ~1500 to 9000 s^{-1} for H_2 oxidation (at pH = 7 and 30 °C)[11] is extremely high, corresponding to a turnover current of ~0.5 to 3 fA per *Av* H_2ase molecule. We have recently reported a protocol for studying *Av* H_2ase PFV on Au by pretreating the surface with the electrode modifier polymyxin (PM).[12] This allows for the subsequent immobilization of an active submonolayer of *Av* H_2ase, which exhibits a highly stable characteristic electrocatalytic behavior. Here we demonstrate PFV measurements on less than 50 *Av* H_2ase molecules immobilized on a nanoelectrode. Extrapolation of the results and analysis presented here suggest that single-enzyme molecule voltammetry is feasible.

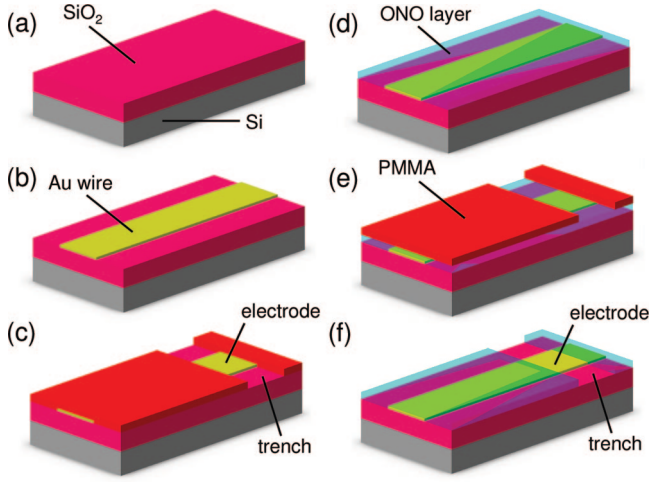

Figure 2. Schematic representation of the process used for the fabrication of micro- and nanosized Au electrodes. The electrodes are insulated using either PMMA (a−c) or a dielectric layer consisting of SiO_2/Si_3N_4/SiO_2 (ONO layer, a, b, d−f).

RESULTS AND DISCUSSION

Fabrication and Characterization of the Electrodes. Our approach for fabricating Au micro- and nanoelectrodes is schematically depicted in Figure 2. Starting from a Si substrate with 500 nm thermally grown SiO_2 (Figure 2a), electron-beam (e-beam) lithography was used to pattern a 30 nm thick Au wire (Figure 2b). This wire had a central region with a nominal width ranging from 50 nm to 5 μm and a length of 300 μm. Outside this central region, the wire was 1 μm in width and extended to macroscopic contact pads 7.5 mm away from the central region. After patterning, the entire Au pattern was insulated with a layer of PMMA. A second e-beam lithography step was then used to remove a narrow trench in this passivation layer that intersected with the narrow Au wire in a perpendicular orientation (Figure 2c). This led to an exposed electrode with a rectangular geometry, its length and width being defined by the width of the trench in the PMMA and by the width of the Au wire, respectively. A minimum PMMA thickness of 300 nm was used (tunable to ±10 nm) since otherwise a large spread was found in the voltammetric response for electrodes smaller than 500 × 500 nm^2, which we attribute to the formation of pinholes. As a final step, an anisotropic O_2 plasma was used to clean the electrode by removing any remaining resist or other organic material from the exposed metal. Further details of the fabrication process are given in the Experimental Section.

As an alternative to PMMA for passivation, we also investigated the use of a dielectric layer obtained by sputtering 10 nm SiO_2/60 nm Si_3N_4/20 nm SiO_2 (ONO layer, Figure 2d). PMMA was then spun unto the wafer, and a narrow trench was lithographically defined in the PMMA (Figure 2e). In a final step, this pattern was transferred to the ONO layer using reactive ion etching (Figure 2f). The PMMA remaining on the ONO layer after the dry etch procedure could also be preserved as additional insulation.

Both fabrication schemes yielded robust and reproducible square Au micro- and nanoelectrodes with nominal sizes ranging from 5 × 5 μm^2 to 100 × 100 nm^2 (using an ONO layer)[15] or 50 × 50 nm^2 (relying solely on PMMA). The insulating qualities of both layers were found to be comparable.

Figure 3 shows scanning electron microscopy (SEM) images of Au electrodes of different sizes. In these images, the horizontal lines correspond to the Au wire, whereas the vertical lines correspond to the trenches in the insulating PMMA layer. To estimate the actual electrode dimensions, the electrodes were exposed under ambient conditions to a solution containing 2.4 mM 1,1′-ferrocenedimethanol ($Fc(MeOH)_2$) as redox mediator and 25 mM NH_4NO_3 as supporting electrolyte. The solution was contained in a PDMS cell with a circular opening (radius ~ 75 μm) at its bottom which was pressed against the surface of the wafer containing the electrode using a micromanipulator. Because of the small currents involved, a two-electrode configuration (without an auxiliary electrode) was appropriate. The fabricated electrode, contacted *via* one of the macroscopic contact pads, was used as working electrode while the reference and auxiliary terminals of the potentiostat were connected to a Ag/AgCl/3 M NaCl reference electrode (+215 mV *versus* NHE) inserted at the top of the PDMS cell. The results of these cyclic voltammetry measurements are also shown in Figure 3. A sigmoidal response with the expected mass-transport-limited current plateau at high potential[5] and the correct half-wave potential for $Fc(MeOH)_2$ (+0.24 V *vs* Ag/AgCl/3 M NaCl) were observed. The Nernstian shape of these curves reflects the fast electron transfer kinetics at the electrode surface. The small capacitive background current measured for the 100 × 100 and 50 × 50 nm^2 electrodes (both ~0.6 pA at 10 mV s^{-1}) is promising for their use in detecting the small currents associated with catalysis by a small number of enzyme molecules.

Modeling of Mass Transport. The value at which the current saturates at high potentials, the so-called diffusion-limited current I_{lim}, is governed by diffusion of $Fc(MeOH)_2$ to the electrode. For a micro- or nanoelectrode in contact with bulk solution, the general steady-state expression for I_{lim} is given by[5]

$$I_{lim} = nFD\Delta C\chi \quad (1)$$

where n is the number of electrons involved in the electrochemical reaction, ΔC the difference between the $Fc(MeOH)_2$ concentration in the bulk and at the electrode surface (in this case, ΔC is equal to the bulk concentration, 2.4 mM), D the diffusion coefficient of $Fc(MeOH)_2$ (6.4 × 10^{-10} m^2 s^{-1}),[16] and χ is a factor that depends solely on the geometry and size of the electrode. For example, a microdisk electrode has $\chi = 4R$ with R the electrode radius.[5]

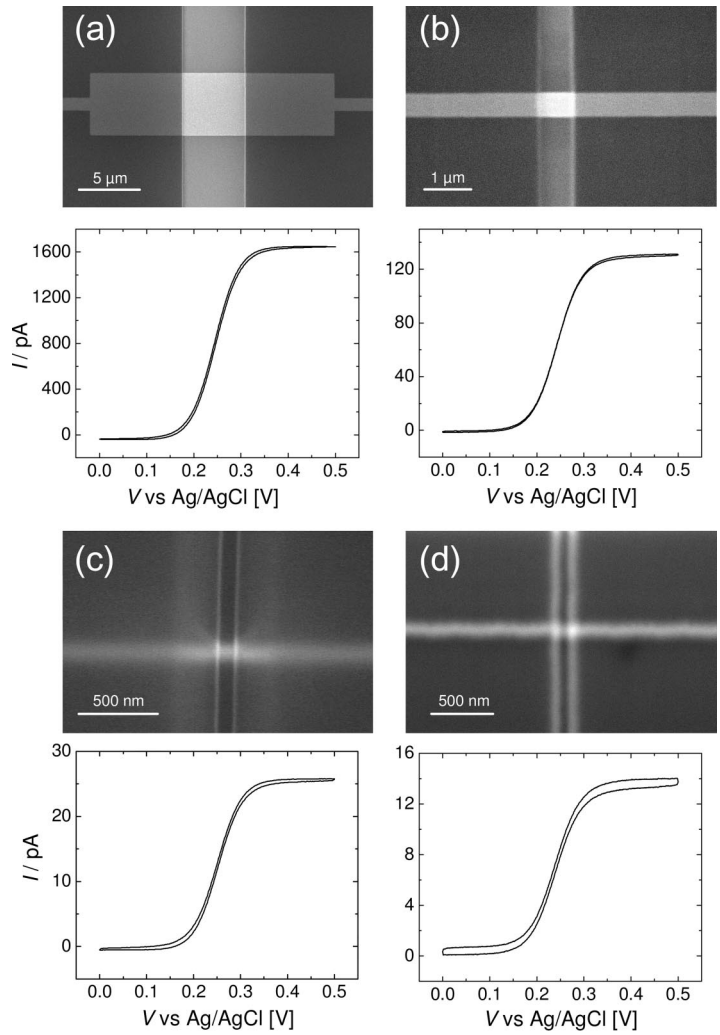

Figure 3. SEM images of fabricated Au electrodes (insulated by a 300 nm thick PMMA layer) and their corresponding electrochemical response when subjected to a solution containing 2.4 mM $Fc(MeOH)_2$ and 25 mM NH_4NO_3: (a) 5 × 5 μm^2; (b) 500 × 500 nm^2; (c) 100 × 100 nm^2; and (d) 50 × 50 nm^2. Scan speed in all cases 10 mV s^{-1}.

For the fabricated electrodes in Figure 3, which have a known geometry, the parameter χ was determined by numerically solving the diffusion equation. The geometry model employed for these calculations is shown in Figure 4a; further details of the calculation method are given in the Experimental Section. A representative result for the concentration profile is shown in Figure 4b in which the radial diffusion pattern, restricted by the side walls of the trench, can be clearly distinguished. The computed values for χ are summarized in Table 1, together with the corresponding limiting currents I_{lim} and the experimentally determined values of I_{lim}. All theoretical values are corrected for the finite simulation volume as discussed in the Experimental Section. An average of 50 electrodes was fabricated for each electrode size, all yielding similar results.

The larger electrodes show good agreement between the calculated and measured values of I_{lim}, whereas for electrodes smaller than 500 nm, these values start to differ. This indicates that the smaller elec-

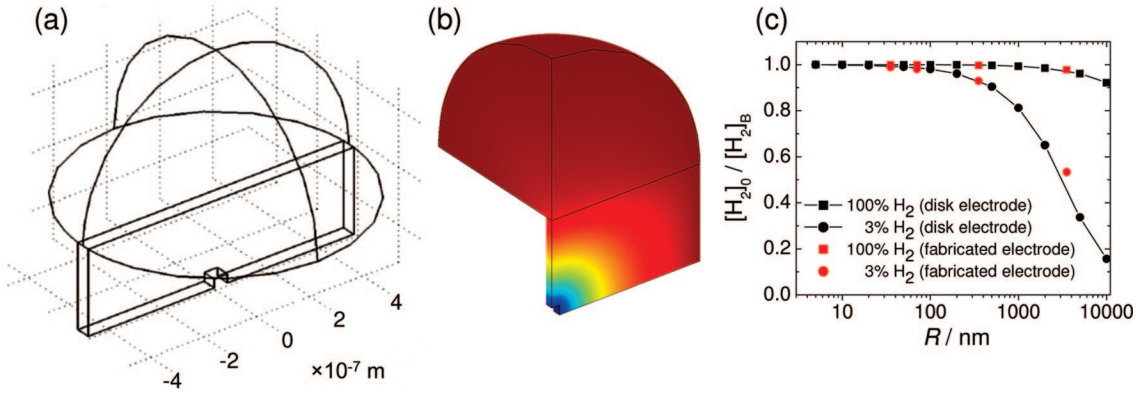

Figure 4. (a) Hemispherical geometry used for theoretical modeling of I_{lim} at a 50 × 50 × 30 nm^3 electrode, located at the bottom of a 300 nm deep trench. (b) Concentration profile for Fc(MeOH)$_2$ obtained by solving the diffusion equation in the geometry depicted in (a). One quarter of the volume of part (a) is shown. The color code indicates the increasing Fc(MeOH)$_2$ concentration, from C = 0 mM at the electrode surface (dark blue) to C = 2.4 mM in bulk solution (dark red). (c) Modeling of the degree of mass transport limitation expected for H_2 oxidation by *Av* H_2ase at ideal Au disk electrodes (black symbols) and the fabricated Au electrodes from Table 1 (red symbols) as a function of electrode size for two different values of $[H_2]_B$. For disk electrodes, the value R of the abscissa represents the electrode radius. For fabricated Au electrodes, R is taken as $1/\sqrt{2}$ times the length of one side. These curves correspond to a fractional enzymatic surface coverage of θ = 0.1. The lines are guides to the eye.

trodes are somewhat larger than designed. For the smallest electrodes in Table 1, the measured value of I_{lim} combined with finite-element modeling suggests that the actual dimensions are closer to 130 × 130 and 70 × 70 nm^2 (assuming equal deviations in length and width). We expect that this discrepancy is due to the trench width deviating somewhat from the designed value. This is suggested by the representative SEM image of a 500 × 500 nm^2 electrode in Figure 3b and may be caused by a combination of the e-beam edge profile and the O_2 plasma cleaning of the electrode liberating additional Au. For electrodes of sizes ≤100 × 100 nm^2, additional broadening of the Au in the lift-off procedure may also contribute.

An important consideration in PFV is that mass transport of substrate to the enzyme molecules should not be rate limiting, as this may distort the observed kinetics. This is particularly challenging when working with enzymes with a high turnover rate such as *Av* H_2ase, for which H_2 oxidation is often limited by mass transport of H_2 to the electrode.[10] An estimate of the mass transport limitation that may occur can be obtained by equating the rate of transport of substrate to the electrode with the catalytic turnover of the protein. For the case of H_2 oxidation[17] by *Av* H_2ase, the following equation (derived in the Supporting Information) holds in the steady state:

$$\frac{[H_2]_0}{[H_2]_B} = 1 - \frac{A\theta}{\chi D A_P N_A [H_2]_B} \frac{k_{max}}{1 + K_M / [H_2]_0} \qquad (2)$$

Here $[H_2]_0/[H_2]_B$ is the steady-state ratio of the H_2 concentration at the electrode surface ($[H_2]_0$) and in the bulk ($[H_2]_B$), which gives a direct indication of any mass transport limitation. This ratio is unity in the absence of such a limitation and tends toward zero with increasingly limiting mass transport. A is the surface area of the electrode (taking into account the specific electrode geometry), A_p the area of the adsorbed protein (38.5 nm^2 as estimated from the crystallographic dimensions[18]), θ the fractional enzymatic coverage of the electrode surface, N_A Avogadro's number, D the diffusion coefficient of H_2 (4.8 × 10^{-9} m^2 s^{-1}),[19] k_{max} the maximum turnover number of the protein (upper estimate 9000 s^{-1}),[11] and K_M the Michaelis−Menten constant for H_2 oxidation by *Av* H_2ase (8 × 10^{-3} mol m^{-3}).[11]

The calculated value of $[H_2]_0/[H_2]_B$ is plotted in Figure 4c as a function of the electrode radius R for an enzymatic surface coverage of θ = 0.1, using either $[H_2]_B$ = 0.8 mol m^{-3} (corresponding to measurements performed under a headspace of 100% H_2) or $[H_2]_B$ = 0.024 mol m^{-3} (corresponding to 3% H_2 in Ar as used in previous studies).[12] To illustrate the behavior of $[H_2]_0/[H_2]_B$ for a wide range of electrode sizes, the results are plotted for hypothetical Au disk electrodes (black symbols). The simulated data for our actual electrode geometry are also shown, for which χ was evaluated numerically. The results for both electrode types are similar. At a fixed $[H_2]_B$ concentration, an increase in the electrode size leads to a decrease of $[H_2]_0$ as diffusion becomes insufficient to keep up with the surface reaction. For an atmosphere containing 3% H_2 in Ar, there appears a significant discrepancy between $[H_2]_0$ and $[H_2]_B$ for elec-

TABLE 1. Calculated *versus* Experimental Values for I_{lim} (Mask Thickness 300 nm)

electrode size [nm^2]	χ [m]	I_{lim} [pA]	I_{lim} [pA]
(design)	(calculated)	(calculated)	(experimental)
5000 × 5000	1.10 × 10^{-5}	1640	1680 ± 19
500 × 500	8.59 × 10^{-7}	127	131 ± 4
100 × 100	1.30 × 10^{-7}	19	26 ± 2
50 × 50	6.02 × 10^{-8}	8.9	13 ± 2

trodes larger than 100 nm. Under an atmosphere of 100% H_2, however, this discrepancy is much less dramatic, as shown for a large electrode size of $R = 1$ μm, where the difference between $[H_2]_0$ and $[H_2]_B$ is still smaller than 1%. Since our experimental setup allows us to work under 100% H_2 and to tune the fabricated electrode size down to ~70 × 70 nm^2, we do not expect mass transport to be an important limitation in our measurements. Moreover, these calculations using $\theta = 0.1$ represent a somewhat conservative estimate of the limitations imposed by H_2 mass transport since we have previously shown that the immobilization of *Av* H_2ase on Au by pretreatment of the Au surface with PM yields a maximum enzymatic surface coverage of electrochemically active molecules of 5.5%.[12]

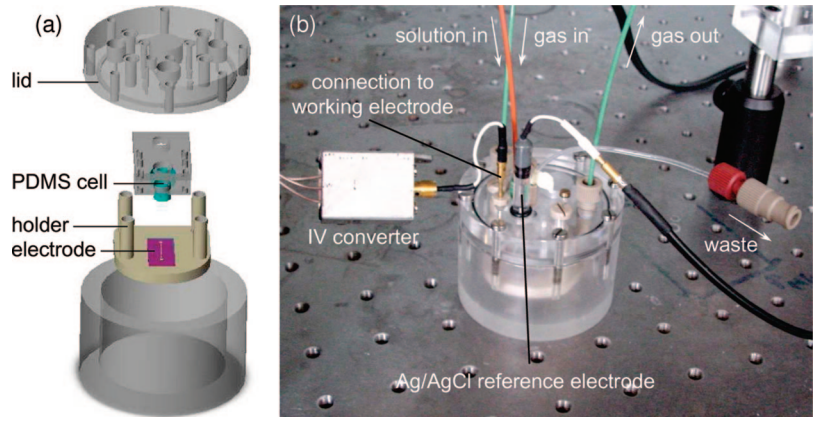

Figure 5. (a) Schematic representation and (b) photograph of a home-built Perspex cell used for performing electrochemical measurements under strict exclusion of O_2.

Protein Film Voltammetry. Having established the fabrication of stable Au nanoelectrodes and having shown the ability to prevent any detrimental mass transfer limitations in our specific electrode geometry, we proceeded to perform PFV using this system. Because the active site of *Av* H_2ase is quickly transformed to an inactive state by the presence of both reducing equivalents and O_2,[7] measurements had to be performed under strict exclusion of O_2. For this purpose, the wafer containing the Au electrode together with a gas-permeable PDMS cell to hold the solution was sealed inside a Perspex gas-flow cell, as illustrated in Figure 5a. An opening in the bottom of the PDMS liquid cell allowed fluid to make contact with the electrode, and oxygen-tight tubing (PEEK) permitted delivering solution to the bottom of the PDMS cell in close vicinity to the working electrode. A second tube removed any waste from the top of the fluid volume. The electrode was contacted *via* a spring-loaded pin which made contact with one of the macroscopic Au pads situated on the wafer. A reference electrode (Ag/AgCl/3 M NaCl) passed through the lid of the Perspex gas cell and made direct contact with the fluid in the PDMS fluid cell. Figure 5b shows the sealed Perspex cell with all liquid, gas, and electrical connections established. A gas mixing system allowed the measurements to be performed under an atmosphere of N_2, Ar, H_2, or any mixture thereof. The headspace of the cell was flushed with the required gaseous mixture until the diminishing O_2 reduction signal at low potential stabilized, enabled by the gas-permeable nature of the PDMS cell. For Ar and N_2, the time needed for complete O_2 removal was determined in a separate experiment to be ~90 min (see the Supporting Information).

We initially performed PFV on macroscopic *Av* H_2ase samples. Au surfaces were prepared by e-beam evaporation of 2 nm Cr followed by 200 nm Au onto freshly cleaved mica. The Au was then pretreated with PM by applying a 10 g L^{-1} solution to the wafer for 30 min, rinsing with water, and drying in a stream of dry N_2. A PDMS cell was subsequently attached to the wafer, thereby defining the working electrode area by the size of the circular opening at the bottom of the PDMS cell (radius ~ 75 μm). After filling with buffer solution (50 mM MES buffer and 100 mM NaCl at pH = 5.7), the cell was mounted inside the Perspex gas-flow cell. A pH of 5.7 was selected since the proton-reduction activity is close to its optimal value[20] while oxidative inhibition is slow.[21,22] After sealing the gas-flow cell, Ar was flushed into its headspace for 2 h to remove O_2; 250 μL of solution (corresponding to the full volume of the PDMS cell) containing *Av* H_2ase in buffer was then injected close to the working electrode. The applied *Av* H_2ase concentration (typically 250 nM) far exceeded the K_d of 35 nM for *Av* H_2ase binding to PM-coated Au.[12] A lag time of 90 min was usually observed during which a small trace of O_2 introduced during sample injection disappeared and the catalytic signal of *Av* H_2ase grew to its full amplitude.[23] The Supporting Information shows cyclic voltammograms for these reference experiments, indicating that, under the experimental circumstances, *Av* H_2ase forms an active submonolayer on PM-pretreated Au. Stable catalytic behavior was observed over a period of days (without continuous potential cycling).

After establishing the viability of the experimental procedure, similar measurements were performed using fabricated 5 × 5 $μm^2$ electrodes (Figure 6). Under Ar, in the absence of H_2 (Figure 6a), a sigmoidal-type proton reduction wave was obtained accompanied by the peak-shaped reoxidation of the accumulated H_2 (the latter only at very low scan rates). This behavior is very similar to that found for *Av* H_2ase immobilized on a stationary edge-plane graphite (EPG) electrode.[7−9] Without the enzyme, no such response was obtained. After switching to an atmosphere of 100% H_2 (Figure 6b), the proton reduction wave was suppressed, as

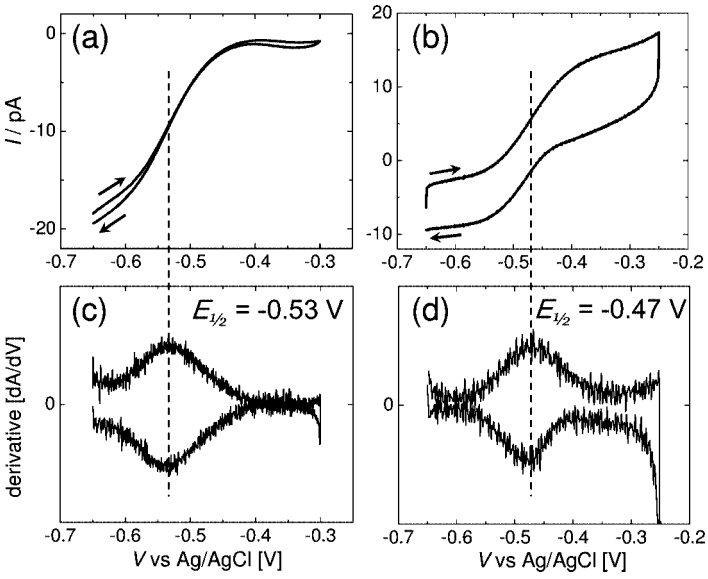

Figure 6. PFV of *Av* H_2ase immobilized on 5 × 5 μm² fabricated Au electrodes (insulated by 300 nm PMMA), pretreated 30 min with 30 g L^{-1} PM. Under an (a) Ar and (b) 100% H_2 atmosphere, the characteristic electrochemical response of *Av* H_2ase is detected. Panels (c) and (d) show the derivatives of the current measured in (a) and (b), respectively, indicating the correct electrochemical half-wave potentials for catalysis by *Av* H_2ase under the applied conditions. The *Av* H_2ase concentration was 200 nM. The buffer contained 50 mM MES buffer and 100 mM NaCl, pH = 5.7. Scan speeds were (a) 1.5 mV s^{-1} and (b) 15 mV s^{-1}.

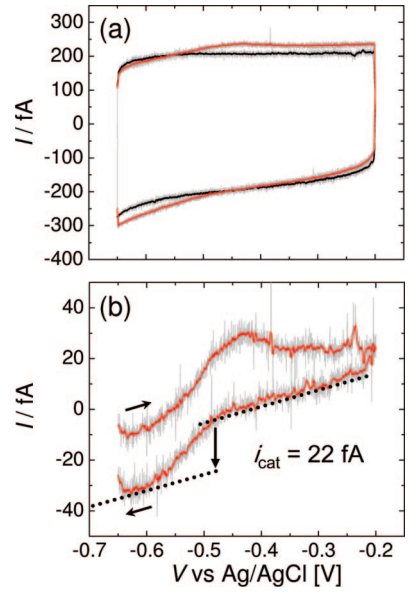

Figure 7. PFV of *Av* H_2ase immobilized on a 100 × 100 nm² (design value) fabricated Au electrode, pretreated 30 min with 30 g L^{-1} PM. The electrode was insulated with an ONO layer. (a) Curves recorded with only buffer (black) and after the introduction of 250 μL of 500 nM H_2ase in buffer (red). (b) Difference between the red and the black curves from (a). The buffer contained 50 mM MES buffer and 100 mM NaCl, pH = 5.7. Scan speed: 1.5 mV s^{-1}. The light gray lines represent the raw data, while the red lines are the same data smoothed over a window of 2 s.

expected,[7−9] and a sigmoidal oxidation wave dominated the voltammogram.

The proton reduction and H_2 oxidation waves exhibited residual slopes at high overpotential, which was observed in all of our *Av* H_2ase PFV measurements. This feature has also been reported on EPG and has been ascribed to dispersion in the interfacial electron transfer rates due to a distribution of tunneling distances resulting from different molecular orientations.[4] Since we are working at pH = 5.7, the turnover currents measured for H^+ reduction and H_2 oxidation are comparable,[20] which confirms that the enzymatic coverage is not significantly altered during the 15 min required to equilibrate the 100% H_2 atmosphere. The observed catalytic activity for H_2 oxidation can be related to the enzymatic surface coverage using a maximum turnover rate[11] of 1500 to 9000 s^{-1}; for a 5 × 5 μm² electrode, this yields an active *Av* H_2ase coverage between 6 and 1%,[24] respectively, consistent with the maximum coverage (~5.5%) deduced from atomic force microscopy data.[12] The midpoint potentials found for H^+ reduction and H_2 oxidation lie above the theoretical H^+/H_2 value (E = −0.55 V at pH = 5.7) and agree with previous results on macroscopic electrodes.[12]

Detecting *Av* H_2ase activity at nanoelectrodes proved much more difficult. Following each experiment, the electrodes were often found to be heavily damaged or destroyed. This was especially pronounced for the smallest electrode sizes. Testing with different supporting electrolytes revealed that the damage was caused by Cl^-, which we did not anticipate based on the negative potentials employed. Unfortunately, as we have clearly shown previously,[12] the presence of Cl^- in solution is imperative for obtaining *Av* H_2ase activity although the reason for this effect remains unknown. Electrodes fabricated with an ONO layer as insulating material proved more resilient to exposure to Cl^-. This is possibly a result of residual contamination from the fabrication process helping to protect the electrodes (but still enabling PM attachment).

Using ONO devices, we were able to measure distinct *Av* H_2ase activity on a 100 × 100 nm² (nominal value) electrode, as shown in Figure 7. The clear sigmoidal reduction wave is followed by the peak-shaped reoxidation of the H_2 produced at low potentials and is strongly reminiscent of *Av* H_2ase PFV on macroscopic electrodes. The shape of the voltammogram resembles our data for macroscopic electrodes, suggesting that it still represents an average over a heterogeneous enzyme molecule population. On the basis of the observed turnover current of 22 fA, we estimate that the cyclic voltammogram is composed of the contributions of ~8 to 46 enzyme molecules (based on k_{max} = 9000 to 1500 s^{-1}, respectively).[24,25] To our knowledge, this represents by far the smallest number of enzyme molecules to have been detected in PFV to date.

CONCLUSIONS

We have developed highly sensitive electrochemical instrumentation aimed at performing single-enzyme molecule electrochemistry on nano-

electrodes. Despite limits imposed by the instability of the electrodes to the chemical environment specifically required for *Av* H_2ase on PM-pretreated Au electrodes, we were able to perform PFV on mesoscopic samples down to less than 50 enzyme molecules. This methodology is applicable to other redox enzymes with high catalytic activity so long as they can be immobilized on Au surfaces. We envision that single-enzyme molecule electrochemistry will become possible in the near future.

EXPERIMENTAL SECTION

Materials. Reagents were purchased from Acros or Aldrich and were used without further purification. Polymyxin B sulfate (PM) was purchased from Sigma (product P1004, predominantly decapeptide B1, $C_{55}H_{96}N_{16}O_{13}\bullet 2H_2SO_4$). PM solutions were stored at −20 °C and generally used for 1 month. *Av* H_2ase was isolated and purified from *Allochromatium vinosum* and optimally activated by 30 min incubation under 100% H_2 at 50 °C.[26] MES (2-(*N*-morpholino)ethanesulfonic acid) buffer (purchased from Sigma) was titrated with NaOH to pH = 5.7. Deionized water (18 MΩ cm Milli-Q, Millipore) was used to prepare all solutions and for rinsing samples and electrodes. The reference electrode was a Ag/AgCl/3 M NaCl electrode (BAS RE-5B), +215 mV *versus* NHE.

Modeling. The expected diffusion-limited current I_{lim} was determined by solving the diffusion equation using a finite-element package (COMSOL) and realistic, three-dimensional geometry models for our devices. The simulation volume encompassed the electrode, the trench on the surface, and a hemispherically shaped region of bulk solution centered on the electrode and with radius R_{hem}. The mesh on the electrode surface was generally taken as 1/100 of the length of one side. As boundary conditions, the $Fc(MeOH)_2$ concentrations at the electrode surface, C_0, and on the outer hemispherical boundary, C_B, were taken as 0 and 2.4 mM, respectively. The value of the diffusion-limited current obtained in this way, $I_{lim(uncorrected)}$, is exact in the limit $R_{hem} \rightarrow \infty$ but is overestimated by ~1% for the values of R_{hem} that we employed. A corrected value $I_{lim(corrected)}$ was obtained using

$$I_{lim(corrected)} = \frac{I_{lim(uncorrected)}}{1 + \frac{I_{lim(uncorrected)}}{2\pi R_{hem} F D C_B}} \quad (3)$$

as discussed in the Supporting Information (all symbols are as in the main text).

Fabrication of the Electrodes. Si wafers with 500 nm SiO_2 were cleaned in nitric acid (5 min ultrasound), rinsed in acetone (1 min), rinsed with *iso*-propanol (IPA), and dried in a stream of dry N_2. A first e-beam step was performed using 950 K PMMA (3% in anisole) spun for 1 min at 3000 rpm, yielding a PMMA layer with a thickness of 150 nm. This layer was prebaked at 175 °C for 10 min. After development of the written pattern with IPA/H_2O 7:3 (60 s) and IPA (stopper, 30 s) and drying in a stream of dry N_2, 1 nm Cr (or, alternatively, 2 nm Ti) and 30 nm Au were evaporated onto the pattern by electron beam evaporation at 10^{-7} mbar using a low evaporation rate of 0.2 Å s^{-1}. When the insulating material consisted of $SiO_2/Si_3N_4/SiO_2$ (ONO layer), an additional 0.5 nm Cr layer was evaporated on top of the Au as a sticking layer. Lift-off was achieved by immersing the patterned wafers in hot acetone (55 °C) for 30 min and subsequent use of ultrasound (40 kHz) for a maximum of 10 s. The samples were then rinsed with IPA and dried in a stream of dry N_2. Longer exposure to ultrasound severely damaged the resulting Au lines, especially for line widths below 500 nm. When using only PMMA as an insulating material, 950 K PMMA (6% in anisole) was spun for 1 min at 6000 rpm, yielding a PMMA layer with a thickness of 360 nm. This layer was prebaked at 175 °C for at least 2 h. When using an ONO layer as insulating material, after the lift-off procedure, 10 nm SiO_2, 60 nm Si_3N_4, and 20 nm SiO_2 were sputtered onto the Au pattern at 1 mTorr. Subsequently, 950 K PMMA (7% in anisole) was spun for 1 min at 3000 rpm, yielding a PMMA layer with a thickness of 650 nm, which was prebaked at 175 °C for 10 min. In both approaches, the second e-beam step liberated the macroscopic contact pads and the electrode. When using only PMMA, this was achieved through development of the written pattern with IPA/H_2O 7:3 (60 s) and IPA (stopper, 30 s) and drying in a stream of dry N_2. For ONO layer devices, similar development and drying steps were used, followed by anisotropic reactive ion etching (RIE) using CHF_3/O_2 (50 sccm CHF_3, 2.5 sccm O_2, 7 μbar, 50 W). The etch end point was determined using optical interference detection, and a 20% overetch was generally used since etching the trench was much slower than liberating the macroscopic contact pads, where the etch process was monitored (etch rates: SiO_2 and Si_3N_4 = 12 nm min^{-1}, Au = 5 nm min^{-1}, and PMMA = 30 nm min^{-1}). The electrodes were finally cleaned by employing an anisotropic O_2 plasma (20 sccm O_2, 3 μbar, 50 W, 30 s) during which ~60 nm PMMA was removed (etch rate PMMA = 120 nm min^{-1}).

Electronics for Electrochemical Measurements. All measurements were carried out in a two-electrode configuration. For PFV measurements on macroscopic electrodes, a commercial potentiostat (model CHI832B, CH Instruments) was used. For measurements on micro- and nanoelectrodes, custom-built electronics were employed. The current at the working electrode was detected using a current−voltage (*IV*) converter consisting of an operation amplifier in the inverting configuration with a gain of either 10^9 or 10^{11} V/A. The voltage output of the *IV* converter was further amplified by a factor 10 or 100 using a separate voltage postamplifier stage. Both the *IV* converter and the postamplifier were powered by chemical batteries and were situated inside a Faraday cage that also housed the electrochemical cell. This system exhibited 2 fA total rms noise and a bandwidth of 3 Hz for a typical load in our experiments. The amplified signal was routed to an input on an ADwin-Gold DAC/ADC interface (Jäger Computergesteuerte Messtechnik, Germany) located outside the Faraday cage. The ADwin-Gold was also used to apply a potential to the reference electrode with respect to the working electrode. All ADC inputs and DAC outputs were filtered using first-order low-pass filters with a cutoff frequency of 30 Hz, as well as π-filters to eliminate logic-frequency interference. The ADwin-Gold was connected to a computer *via* a USB interface and controlled using in-house LABview software.

Acknowledgment. We acknowledge assistance from D. Krapf in the early stages of the experiment. This work was financially supported by The Netherlands Organization for Scientific Research (NWO).

Supporting Information Available: Derivation of eqs 2 and 3. Decrease of the O_2 concentration in the cell as a function of time (Figure S1). PFV reference experiments of *Av* H_2ase on PM-pretreated Au-covered mica (Figure S2). This material is available free of charge *via* the Internet at http://pubs.acs.org.

REFERENCES AND NOTES

1. For a recent review, see: Walter, N. G.; Huang, C.-Y.; Mano, A. J.; Sobhy, M. A. Do-It-Yourself Guide: How to Use the Modern Single-Molecule Toolkit. *Nat. Methods* **2008**, *5*, 475–489.
2. For a recent comprehensive review, see: Léger, C.; Bertrand, P. Direct Electrochemistry of Redox Enzymes as a Tool for Mechanistic Studies. *Chem. Rev.* **2008**, *108*, 2379–2438.
3. Armstrong, F. A.; Heering, H. A.; Hirst, J. Reaction of Complex Metalloproteins Studied by Protein-Film Voltammetry. *Chem. Soc. Rev.* **1997**, *26*, 169–179.

4. Léger, C.; Jones, A. K.; Albracht, S. P. J.; Armstrong, F. A. Effect of a Dispersion of Interfacial Electron Transfer Rates on Steady State Catalytic Electron Transport in [NiFe]-Hydrogenase and Other Enzymes. *J. Phys. Chem. B* **2002**, *106*, 13058–13063.
5. Bard, A. J.; Faulkner, L. R. *Electrochemical Methods: Fundamentals and Applications*, 2nd ed.; John Wiley & Sons: New York, 2000.
6. Arrigan, D. W. M. Nanoelectrodes, Nanoelectrode Arrays and Their Applications. *Analyst* **2004**, *129*, 1157–1165.
7. Vincent, K. A.; Parkin, A.; Armstrong, F. A. Investigating and Exploiting the Electrocatalytic Properties of Hydrogenases. *Chem. Rev.* **2007**, *107*, 4366–4413.
8. De Lacey, A. L.; Fernandez, V. M.; Rousset, M.; Cammack, R. Activation and Inactivation of Hydrogenase Function and the Catalytic Cycle: Spectroelectrochemical Studies. *Chem. Rev.* **2007**, *107*, 4304–4330.
9. Lubitz, W.; Reijerse, E.; van Gastel, M. [NiFe] and [FeFe] Hydrogenases Studied by Advanced Magnetic Resonance Techniques. *Chem. Rev.* **2007**, *107*, 4331–4365.
10. Jones, A. K.; Sillery, E.; Albracht, S. P. J.; Armstrong, F. A. Direct Comparison of the Electrocatalytic Oxidation of Hydrogen by an Enzyme and a Platinum Catalyst. *Chem. Commun.* **2002**, 866–867.
11. Pershad, H. R.; Duff, J. L. C.; Heering, H. A.; Duin, E. C.; Albracht, S. P. J.; Armstrong, F. A. Catalytic Electron Transport in *Chromatium vinosum* [NiFe]-Hydrogenase: Application of Voltammetry in Detecting Redox-Active Centers and Establishing That Hydrogen Oxidation Is Very Fast Even at Potentials Close to the Reversible H^+/H_2 Value. *Biochemistry* **1999**, *38*, 8992–8999.
12. Hoeben, F. J. M.; Heller, I.; Albracht, S. P. J.; Dekker, C.; Lemay, S. G.; Heering, H. A. Polymyxin-Coated Au and Carbon Nanotube Electrodes for Stable [NiFe]-Hydrogenase Film Voltammetry. *Langmuir* **2008**, *24*, 5925–5931.
13. Volbeda, A.; Garcin, E.; Piras, C.; De Lacey, A. L.; Fernandez, V. M.; Hatchikian, E. C.; Frey, M.; Fontecilla-Camps, J. C. Structure of the [NiFe] Hydrogenase Active Site: Evidence for Biologically Uncommon Fe Ligands. *J. Am. Chem. Soc.* **1996**, *118*, 12989–12996.
14. Kellers, P.; Ogata, H.; Lubitz, W. Purification, Crystallization and Preliminary X-ray Analysis of the Membrane-Bound [NiFe] Hydrogenase from Allochromatium vinosum. *Acta Crystallogr. F* **2008**, *64*, 719–722.
15. Since the dry etch was found to proceed slower through the small trench than to the much larger contact pads, we did not succeed in creating electrodes with trenches smaller than 100 nm because the discrepancy in etching speed became so big that either the contact pads were lost or the nanoelectrode simply could not be liberated. This may be avoided by using separate lithography steps for the trench and contact pads.
16. Zhang, W.; Gaberman, I.; Ciszkowska, M. Effect of the Volume Phase Transition on Diffusion and Concentration of Molecular Species in Temperature-Responsive Gels: Electroanalytical Studies. *Electroanalysis* **2003**, *15*, 409–413.
17. A similar calculation is possible for H^+ reduction, which we have primarily measured; however, the value of K_M is unknown for H^+ reduction by *Av* H_2ase.
18. Fontecilla-Camps, J. C.; Volbeda, A.; Cavazza, C.; Nicolet, Y. Structure/Function Relationships of [NiFe]- and [FeFe]-Hydrogenases. *Chem. Rev.* **2007**, *107*, 4273–4303.
19. Jähne, B.; Heinz, G.; Dietrich, W. Measurement of the Diffusion Coefficients of Sparingly Soluble Gases in Water. *J. Geophys. Res.* **1987**, *92*, 10767–10776.
20. Léger, C.; Jones, A. K.; Roseboom, W.; Albracht, S. P. J.; Armstrong, F. A. Enzyme Electrokinetics: Hydrogen Evolution and Oxidation by *Allochromatium vinosum* [NiFe]-Hydrogenase. *Biochemistry* **2002**, *41*, 15736–15746.
21. Jones, A. K.; Lamle, S. E.; Pershad, H. R.; Vincent, K. A.; Albracht, S. P. J.; Armstrong, F. A. Enzyme Electrokinetics: Electrochemical Studies of the Anaerobic Interconversions between Active and Inactive States of *Allochromatium vinosum* [NiFe]-Hydrogenase. *J. Am. Chem. Soc.* **2003**, *125*, 8505–8514.
22. De Lacey, A. L.; Fernandez, V. M.; Rousset, M. Native and Mutant Nickel-Iron Hydrogenases: Unravelling Structure and Function. *Coord. Chem. Rev.* **2005**, *249*, 1596–1608.
23. This is slower than what we previously observed; it is therefore possible that some reductive reactivation is initially needed after introduction of a small trace of O_2 during sample injection. *Av* H_2ase not bound to PM-treated Au was not flushed out and therefore still present in solution; we do not expect any perturbation of the measured curves because of this.
24. The relatively large error in fractional enzymatic surface coverage is the consequence of the large uncertainty in the experimentally determined value for the maximum turnover number for *Av* H_2ase (k_{max} = 1500 to 9000 s^{-1}).[11] Furthermore, these numbers have been determined at 30 °C and pH = 7, whereas we are working at room temperature (~20 °C) and pH = 5.7. We believe that lowering the temperature to 20 °C (approximately halving the enzymatic activity)[7] while working at pH = 5.7 (approximately doubling the H^+ reduction activity)[7] does not introduce any significant discrepancy.
25. Alternatively, using the maximum enzymatic coverage of 5.5% established for PM-pretreated Au, ~14 enzyme molecules would be present on a 100 × 100 nm^2 electrode, giving k_{max} = 4900 s^{-1}.
26. Coremans, J. M. C. C.; van der Zwaan, J. W.; Albracht, S. P. J. Distinct Redox Behaviour of Prosthetic Groups in Ready and Unready Hydrogenase from *Chromatium vinosum*. *Biochim. Biophys. Acta* **1992**, *1119*, 157–168.